Vol. 20, No. 1 (2021) 227-237
Materiales
Revista Mexicana de Ingeniería Química

Effect of the manufacturing parameters on the quality of the ceramic thermal barrier coating after ageing by thermal treatment

Efecto de los parámetros de manufactura en la calidad del recubrimiento cerámico de barrera térmica después de envejecido por tratamiento térmico

S. Bravo[1], J. Torres-González[2], J. Morales-Hernández[2], E. Martínez-Franco[3], J.C. González-Olvera[4], F.E. Mercader-Trejo[4], A. Rodríguez-López[4], A. Manzano-Ramírez[5], A. Esparza[6], R. Herrera-Basurto[7]*

[1] *Universidad Aeronáutica en Querétaro, Carretera estatal 200 Querétaro-Tequisquiapan No. 22154 Colón, Querétaro, México, C.P. 76270.*

[2] *Centro de Investigación y Desarrollo Tecnológico en Electroquímica, Parque Tecnológico Querétaro s/n, Sanfandila, Pedro Escobedo, Qro., México, C.P. 76703.*

[3] *Centro de Ingeniería y Desarrollo Industrial, Av. Playa Pie de la Cuesta No. 702. Desarrollo San Pablo. Querétaro, Qro. México, C.P. 76125.*

[4] *Universidad Politécnica de Santa Rosa Jáuregui, km 31 + 150 Carretera Federal 57, Santa Rosa Jáuregui, Querétaro, Qro. C.P. 76220.*

[5] *Centro de Investigación y Estudios Avanzados del IPN-Querétaro, Libramiento Norponiente #2000, Fracc. Real de Juriquilla. C.P. 76230 Santiago de Querétaro, Qro. México.*

[6] *Centro Nacional de Metrologia, km 4.5 Carr. A los Cués, EL Marqués Querétaro, Qro.*

[7] *Universidad Tecnológica de Querétaro, División Industria - Nanotecnologías, Av. Pie de la Cuesta 2501, Nacional, 76148 Santiago de Querétaro, Qro.*

Received: May 18, 2020; Accepted: September 1, 2020

Abstract

Deposition parameters effect such as projection distance and argon gas flow as carrier gas on the consistency and thickness of the thermally grown oxide (TGO) layer obtained by plasma thermal spray were studied. In addition, an aging heat treatment without a protective atmosphere was performed to determine the thermal barrier's performance. The thickness of the anchor coating and ceramic coating was characterized by the evolution of the TGO layer by optical microscopy, SEM microscopy, elemental mapping analysis, GDS, and nano-indentation. The results showed that the parameters used to manufacture sample M3, allow a coating with high densification and resistance to thermal fatigue. With the deposition of optimal particles in size and morphology, it is possible to control the diffusion of oxygen and aluminum, which prevents oxygen from moving towards the junction coating and aluminum towards the ceramic joint interface. Thus, control is achieved in the formation of TGO. Also, results indicate that TGO does not exceed the critical limit.

Keywords: manufacturing parameters, quality, ceramic coating.

Resumen

Se estudió el efecto de los parámetros de deposición tales como la distancia de proyección y el flujo de gas argón como gas portador en la consistencia y espesor de la capa de óxido crecido térmicamente (TGO) en una barrera térmica fabricada por proyección térmica asistida por plasma (APS). Después, se realizó un tratamiento térmico de envejecimiento sin atmósfera de protección para conocer el rendimiento de la barrera térmica. Se caracterizó el espesor del recubrimiento de anclaje y del recubrimiento cerámico, así como la evolución de la capa de TGO a través de microscopía óptica, microscopía de barrido con electrones, análisis por mapeo elemental, espectroscopia fotoelectrones y nanoindentación. Los resultados mostraron que los parámetros empleados en la fabricación de la muestra M3, permiten un recubrimiento con alta densificación y con alta resistencia a la fatiga térmica. Con la deposición de partículas óptimas en tamaño y morfología se logra controlar la difusión de oxígeno y aluminio. Así se evita que el oxígeno se desplace hacia el recubrimiento de unión y el aluminio hacia la interface de la unión cerámica, y con ello, se logra el control en la formación de TGO. Los resultados indican que TGO no excede el límite crítico.

Palabras clave: parámetros de manufactura, calidad, recubrimiento cerámico.

* *Corresponding author. E-mail*: raul.herrera@uteq.edu.mx
Tel. + 52 442 37 36 925
https://doi.org/10.24275/rmiq/Mat1041
ISSN:1665-2738, *issn-e*: 2395-8472

1 Introduction

Thermal barrier coatings (TBC's) have been considered an alternative resource to extend the life of parts subjected to extreme heat (Ramirez Hernández A., et-al, 2020). Especially all those components that are part of the combustion zones in gas turbines, materials exposed to high temperatures, corrosion and, heavy usage (Stecura, S.; Leibert, C.H. 1977; Armengol González, S. 2006; Chen, W.R. *et al.* 2006; Clarke, D. R. 2012). The mentioned systems have attracted the attention of technical and scientific fields. They represent potential affordable solutions for economic and environmental problems present in different productive sectors, such as power production, aerospace and, automotive industries (Schweda, M. *et al.* 2015, J. Miller, R.A. 1984). In general, TBC's are complex systems formed by several overlapped layers coatings, where each of these surfaces performs specific functions in order to provide particular isolation and protection properties (Vine, R.W., *et al.* 1989; Tsipas, S.A., *et al.* 2004; Salgado-Delgado A. *et al.* 2020).

The coatings must meet a series of requirements to satisfy the environmental needs of temperature and corrosion. Therefore, the first essential quality that a TBC's must-have is a low thermal conductivity. Second, the coating must withstand high elastic stresses and thermofluency, because the components are subject to thermal cycles under stress. The ceramic protection of the blades consists of covering them with a layer of a ceramic material that resists the thermal cycles, working as an insulator to reduce the damage on the base metal. In this sense, TBC's are composed of zirconium oxide (ZrO_2) partially stabilized with yttrium oxide (Y_2O_3).

TBC's system is formed by a Ceramic Top Coat (CTC), composed explicitly by zirconium (ZrO_2) stabilized with yttrium (7-8 wt% Y_2O_3), and a metallic bond coating (MCrAlY), M may be Ni, Co, and Fe, is previously deposited on the metallic substrate. The bond coating plays two leading roles, namely adherence between the ceramic surface and the substrate and, source of aluminum to produce an intermediate layer coating of α-Al_2O_3 called Thermally Grown Oxide (TGO) (García Martínez, M. 2012; Levi, C.G. *et al.*, 2003). Figure 1 shows a general scheme of the different constituents that conform to the thermal barrier.

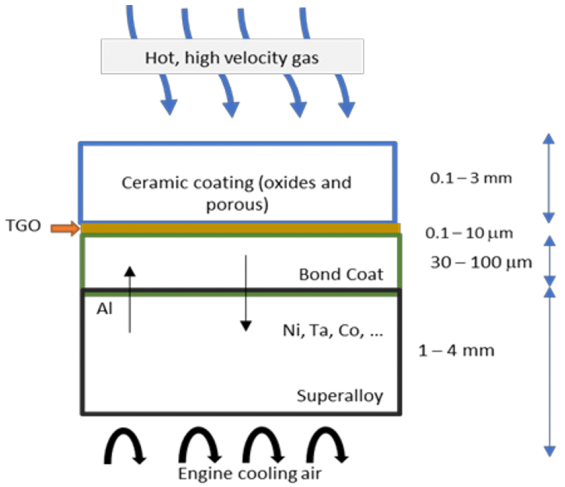

Fig. 1. Scheme of the constituent layers coatings for thermal barriers coatings (TBCs) [5].

A literature review (Stecura, S. *et al.* 1984, Levi, C.G. *et al.* 2003, Manning Meier *et al.* 1991) point out of the studies conducted in the TBC's on their characteristics and properties, none of them indicates or proposes criteria for the quality of the TBC's. Atmospheric plasma spray uses an electric arc to ionize the flowing process gases. The hot gas stream is controlled to melt a wide range of powder feedstock materials to apply high-quality coatings of metals, alloys, carbides, cermets, and oxide ceramics. Atmospheric plasma spray coatings are used for many different applications, including bond coats, corrosion coatings for many different service environments and temperatures, wear coatings, restoration coatings, and thermal barrier materials. The plasma spray process's flexibility comes from its ability to develop sufficient energy to melt almost any coating feedstock material in powder form. The plasma gun (Figure 2, BRO-0006.6 - Atmospheric Plasma Spray Solutions - March 2016), utilizes a chamber with one or more cathodes (electrodes) and an anode (nozzle). With process gases flowing through the chamber, direct current power is applied to the cathode, which arcs to the anode. The powerful arc strips the gas molecules of their electrons to form a plasma plume. As the unstable plasma ions recombine back to the gaseous state, a high thermal energy level is released. The feedstock material is injected into the hot gas, where it is melted and propelled towards the substrate to form the coating.

The process gases typically used are argon, hydrogen, nitrogen, and helium, either individually or in mixtures of two or even three of these gases.

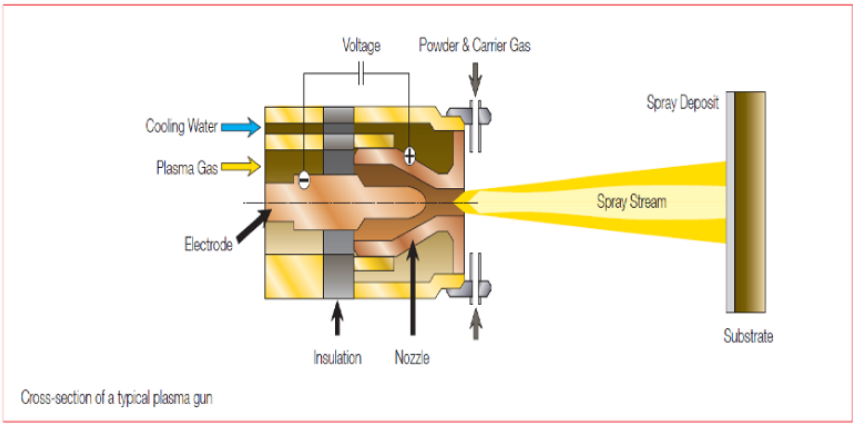

Fig. 2. Typical atmospheric plasma spray gun.

By all the advantages mentioned above, atmospheric plasma-assisted thermal spray process (APS) was explored for the deposition of zirconium and NiCrAlY powders inside the TBC's configuration.

In the present document, the effect of the projection distance and argon flow with the TBC's consistency and their answer to the formation of the Thermally Grown Oxide (TGO) is described. Techniques such as scanning electron microscopy and microanalysis, glow discharge spectroscopy (GDS) and, nano-indentation were used to characterize the samples.

2 Materials and methods

2.1 Coatings deposition

PWA 1375 and CPW 369 specifications were used as a reference to select the feedstock powders for the preparation of ceramic layer and bond coating, respectively. Test pieces were prepared according to the specifications by Pratt & Whitney Aircraft PWA 1375 (Reed, R. C.). Metco 443 NS powder was the bond coating material, composed of a NiCrAlY mixture with a particle size distribution of -125 +45 μm and irregular morphology. Metco 204 NS powder was used for the ceramic layer coating, a material based on zirconium oxide stabilized with yttrium oxide with a particle size distribution of -140 +10 μm, spherical morphology and density of 5.4 g/cm^3. The base material used for the deposition of TBC's was Inconel 625 TM.

Sulzer Metco DJ2700 Hybrid HVOF equipment, configurable for multiple spray processes including atmospheric plasma spray with plasma gun 9MBM, was employed for coatings preparation; the deposition speed was controlled through a 6-axis Kuka KRC2 robot arm. Table 1 shows the variables used in the manufacturing process for each sample, considering that the projection distance (PD) and argon flow (AF) as the main variables for discussion.

The samples thus obtained were identified as M1 and M2, for conditions 1 (same argon flow of 1.981 m^3/h and a different projection distance of 82.55 and 76.20 mm respectively) and, M3 and M4 correspond to conditions 2 (same argon flow of 1.698 m^3/h and a distinct projection distance of 82.55 and 76.20 mm respectively).

Table 1. Experimental parameters for each condition.

Parameter	Sample M1	Sample M2	Sample M3	Sample M4
Argon flow (m^3/h)	1.981	1.981	1.698	1.698
Projection distance (mm)	82.55	76.2	82.55	76.2
Arc Current (A)	600	600	600	600
Plasma Gun	732 A	732 A	732 A	732 A
Air pressure (Kg/cm^2)	5.62	5.62	5.62	5.62
Air pressure at vibrator (Kg/cm^2)	1.05	1.05	1.05	1.05

2.2 *Thermal treatments (ageing)*

Thermal treatment at 1000 °C for 100 and 700 h to observe the effect of fatigue of the TBC's as a function of the projection distance and argon flow was designed. As the aging time was increased, the thickness of the aluminum oxide layer was expected to increase due to the diffusion conditions for its formation being more favored. Thermal treatments were carried out in a Felisa muffle, which is built-in with alumina-silica refractory devices. Oven housing dimensions are 12 x 19 x 11 cm, and the highest allowable temperature and muffle power are 1100 °C and 3000 W, respectively. The oven parameters were set up and monitored using the digital LCD included in the oven.

2.3 *Characterization*

Carls Zeiss optical microscope Axion model was used to observe ceramic and bond coatings' microstructure and morphology. Images were analyzed using free software Image J.

JEOL JSM Scanning Electron Microscope, 6510 model, was used to obtain micrographs, using secondary and backscattering electrons. The cross-sections allowed the validation of the thickness of each coating by SEM. The coatings composition and mapping were determinate by a dispersive energy X-ray (EDX) apparatus attached to the SEM. Compositions profiles were characterized by Glow Discharge Spectroscopy technique (GDS), using a HORIBA Scientific equipment, GD-Profiler 2 model with 35 W of power, and depth resolution of 1 nm.

A nanoindentation tester durometer equipped with Vickers diamond indenter (136°) was used to perform nanoindentation assays. Test procedures and conditions used for depth-sensing nanoindentation experiments were established based on norm ISO 14577-1. The applied load during experiments was 30 μN. According to the Lankford model, fracture toughness was calculated using Young's modulus and Martens hardness determined by nanoindentation results.

3 Results and discussion

3.1 *Microstructural and morphological evaluation*

The microstructural and morphological evaluation of the TBC's was focused on determining the predominant microstructure, the type and number of defects at a selected area; also, and the interactions between the TGO interface and the bond coating were analyzed. The images were obtained through an optical microscope (OM), using bright field, darkfield, and polarized observation modes.

Figure 3 shows microphotographs of M1 acquired by OM, using the sample without any treatment as a reference, at two different modes: (a) bright field and (b) dark area. Bright-field image (Figure 3a) contrasts the bond and top coatings with respect to the substrate, showing a high porosity level and few adherences between the bond coating and the substrate.

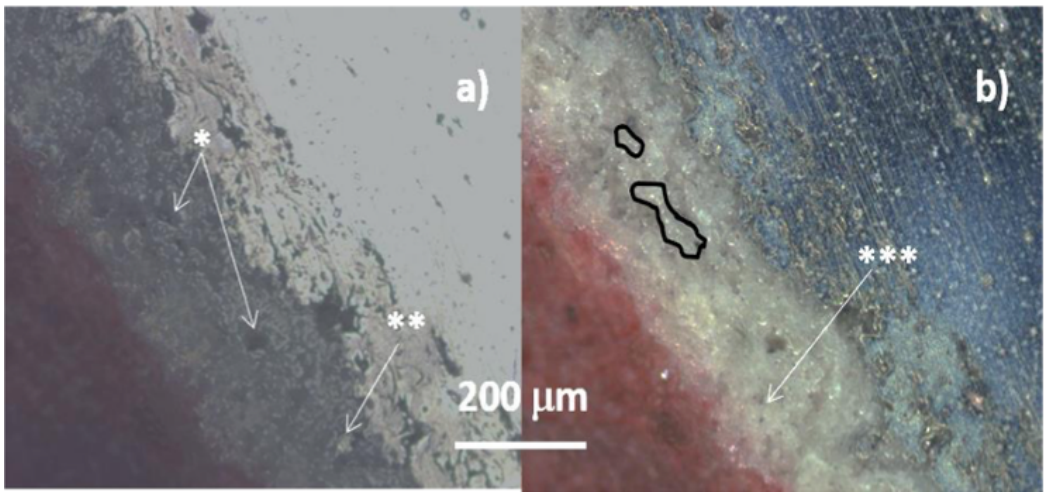

Fig. 3. Coating thickness of each layer (ceramic, bonding and TGO) for both conditions.

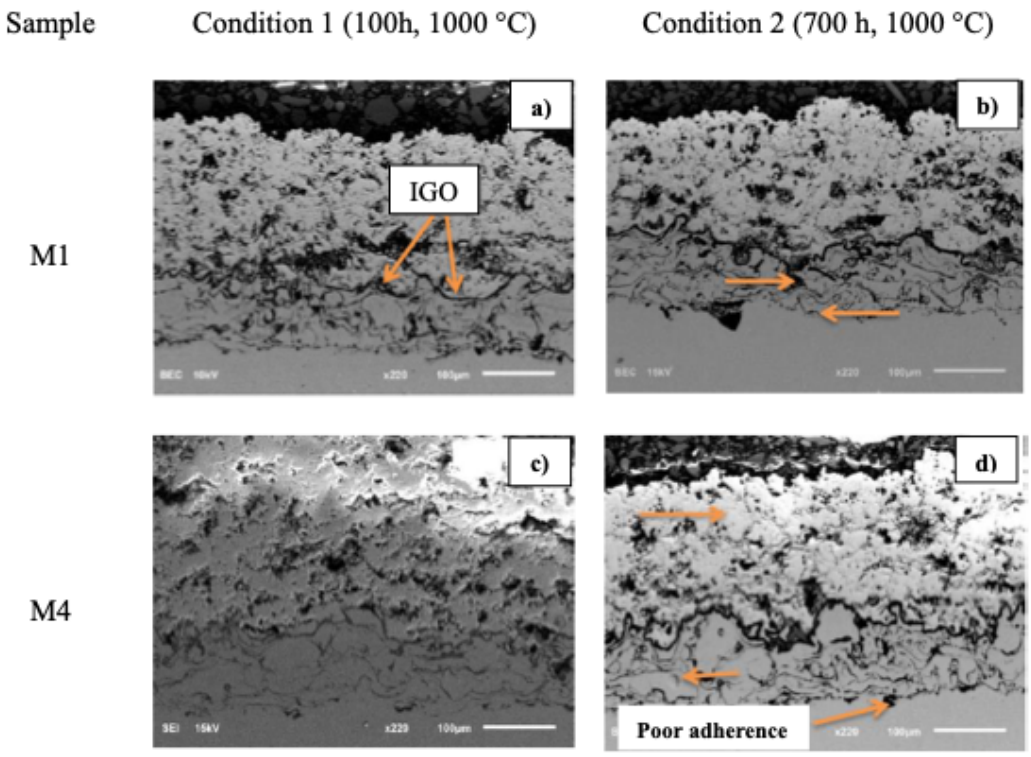

Fig. 4. Micrographs by OM at 200X with polarized light with ageing at 1000 °C during 100 h (Condition 1-T1) and 700h (Condition 2-T2) of treatment.

The darks field imagen shows porosity, unmelted material, and oxides (chromium and nickel oxides) produced during layers coatings deposition were observed (Fig. 3b). The quantity of these three last elements was used as quality criteria for the TBC's. The analysis performed on the TBC's from the samples M1 and M4 that, have been thermally treated (ageing at 1000 °C for 100 and 700 h of treatment) are shown in figure 4. These samples were selected because correspond with the high and low argon flow and with the long and short projection distance, respectively. According with the results in table 3, for the sample M1, the thickness gradient for ceramic coating reported an expansion; the thickness gradient for bond coating showed a compaction and the thickness gradient of IGO was expanded. Micrographs by SEM between the conditions 1 and 2 from M1 sample (Figure 4), shows an increase of IGO and ceramic porosity. The bond coating shows poor adherence with the substrate for both conditions, due to the limited diffusion between them, independent of the ageing time. For the sample M4, the thickness gradient for ceramic coating reported a reduction; the thickness gradient for bond coating showed an expansion and the thickness gradient of IGO was expanded. According to these images, the morphology and microstructure did not change after heat treatment. At the maximum aging time (700 h), the TBC's were denser in all cases and shows a laminar reordering with the formation of secondary phases. With greater projection distance, the TBC's show a more irregular profile.

Less argon flow affects the reduction of plasma, which means a significant energy reduction. However, the pores density and unmelted material at the interphase of each coating (bond coat and top coat) did not show substantive changes before and after aging treatment. Figure 5 shows the thickness of each layer of TBC's from the treated samples. The thickness of each coating was affected by the selection of the manufacturing parameters.

The thickness of the ceramic coating (Figure 5a) was proportional to the projection distance; less projection distance corresponds with less thickness as is observed between the samples M1 vs. M2 and M3 vs. M4.

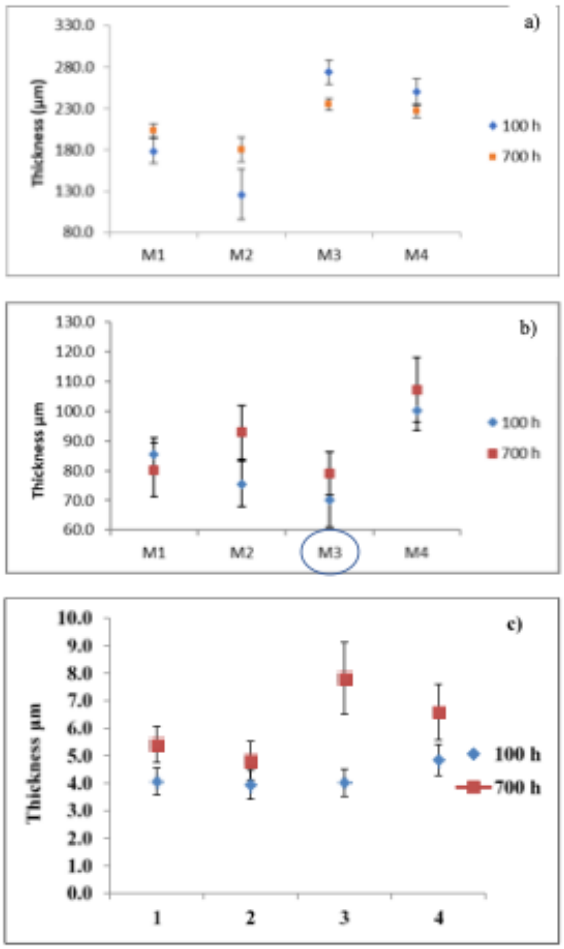

Fig. 5. Micrographs by OM at 200X with polarized light with ageing at 1000 °C during 100 h (Condition 1-T1) and 700h (Condition 2-T2) of treatment.

Less argon flow corresponds with higher ceramic thickness, as shown between the specimens M1 vs. M3 and M2 vs. M4. The effect of aging time for the samples with more argon flow (M1 and M2) shows an increase of thickness like a thermal expansion with an addition in the processing time. When the argon flow was reduced (M3 and M4), increased aging time showed a reduction of the ceramic thickness like a coating sintering, which represents greater diffusion and the possible reduction of porosity. The thickness of the bond coating (Figure 5b) was slightly inversely proportional to the projection distance; less projection distance corresponds with more thickness as is observed between the samples M1 vs. M2 and M3 vs. M4, being more evident in the samples M3 and M4. Less argon flow corresponds with more bonding coating thickness, as is shown between the specimens M1 vs. M3 and M2 vs. M4.

Table 2. Coating thickness of each layer (ceramic, bonding and TGO) for both conditions.

	Ceramic Thickness [μm]	**Bonding Thickness [μm]**	**TGO Thickness [μm]**
Condition 1 (T1, 100 h, 1000 °C)			
M1	166.3	87.1	5.4
M2	114.9	78.9	5.1
M3	335.2	77	5.5
M4	310.8	91.2	6.5
Condition 2 (T2, 700 h, 1000 °C)			
M1	178.4	80.4	9.2
M2	170.3	99.6	7.2
M3	265.6	81.7	7.4
M4	260.9	94.1	8.8

When the aging time increases, the bonding coating thickness increases for all the samples, being more evident with less argon flow and less projection distance (sample M4). The thickness of the Thermally Grown Oxide (TGO) layer (Figure 5c) was proportional to the projection distance; less projection distance corresponds with less thickness as observed between the samples M1 vs. M2 and M3 vs. M4. Less argon flow compare with higher TGO thickness as it is shown between the specimens M1 vs. M3 and M2 vs. M4. The effect of aging time for all the samples shows an increase of TGO thickness like a thermal expansion with the rise in the processing time, being more evident with less argon flow and more projection distance (sample M3).

Table 2 shows the coating thickness of each layer of all samples with 100 and 700 h of aging treatment (Condition 1 and condition 2, respectively). The TBC's thermal stability is an engineering factor of great relevance together with the oxidation resistance and the few formations of the TGO, reducing the aluminum migration from the bond coating to the top layer, and with this, the TBC's embrittlement. The sample M3 reported the less oxidation gradient between the 100 and 700 h of aging treatment.

3.2 Studies of aluminum and oxygen diffusion in different layers

Micrographics obtained with backscattering electrons and basic mapping techniques, corresponding to the sample M4 with 100 h (left) and 700 h (right) of aging treatment, are shown in Figure 6. These microphotographs, it is possible to observe the exact

distribution of the coatings constituting the thermal barrier. The brightest corresponds to the ceramic layer, whereas the bond coating presents a similar intensity than those for the base material layer (Inconel 625 TM). The images obtained, along with the additional elements, provide a clear picture of the interfaces formed between the coatings and the characteristics thereof.

Higher concentrations of aluminum and oxygen present at the interphase between the ceramic and bonding coatings indicate the thermally grown oxide (TGO) layer formation. The diffusion of aluminum through layers was remarkable since this element originated in the bond coating; conversely, oxygen aligns near the ceramic layer, which suggests that it comes from the ceramic coating.

Mapping images, Figure 7, for sample M3-T2, represents a detailed picture of the interaction between Al and O_2 at the interphase between the ceramic and bonding coatings, which are interpreted as the width of the TGO.

Volume changes by the effect of the thermal treatment temperature and time, in the coatings that conform the TBC's, are associate with a porosity reduction, recovery, and recrystallization of their microstructure, as well as the diffusion of some elements toward zones of less concentration for the formation of new compounds (Al_2O_3, e.g.). This means that the coatings were able to expand or contract by the effect of the aging treatment. The thickness gradient of the layers between 100 and 700 h of treatment, is shown in table 3. The minimum thickness gradient of TGO correspond with the sample M3 (Δ= 1.9 μm) where the ceramic coating had the most densification and reduction of the thickness (Δ= -69.6 μm), and the bonding coating had an intermediate expansion (Δ= 4.71 μm) for the others samples.

Interpretation of the elemental maps supports the diffusion of Al towards the ceramic layer, which shows the compatibility of the material used as an anchorage coating. GDS obtained concentrations profiles from the samples M1 and M3 under the conditions T1 and T2, to get more accurate and specific information about mobility of elements through the TGO and neighboring areas, shown in Figure 8. For the sample M1-T1, the oxygen concentration increases at the ceramic-bonding interphase and decreases into the bonding coating. Aluminum concentration was high and homogeneous at the bonding coating. With more aging time, the sample M1-T2 shows a significant reduction of the aluminum and oxygen concentration at the bonding coating for M1-T1.

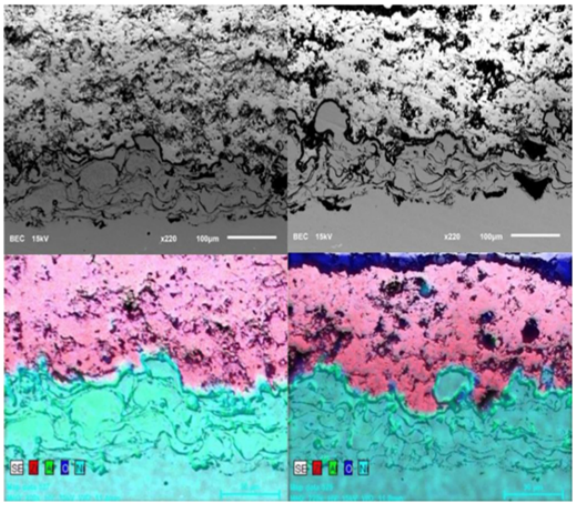

Fig. 6. Microstructure and mapping of the layers constituting the TBC's, correspond to M4-T1 (left) and M4-T2 (right).

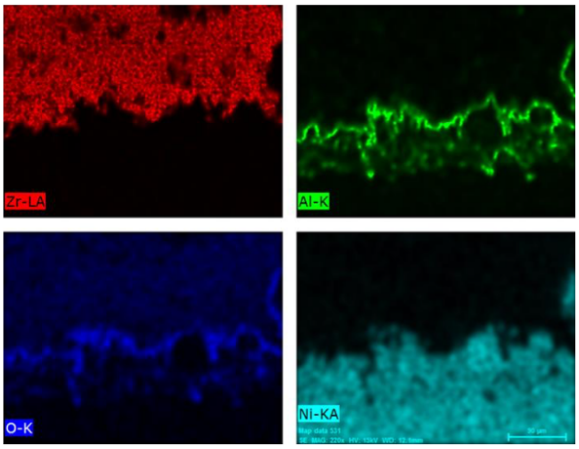

Fig. 7. Elemental mapping for sample M3-T2, after 700 h of treatment.

Table 3. Thickness gradient of the coatings between 100 and 700 h of treatment.

	Thickness Gradient of Ceramic [μm]	**Thickness Gradient of Bonding [μm]**	**Thickness Gradient of TGO [μm]**
M1	12.1	-6.7	3.8
M2	55.4	20.7	2.1
M3	-69.6	4.71	1.9
M4	-49.9	2.9	2.3

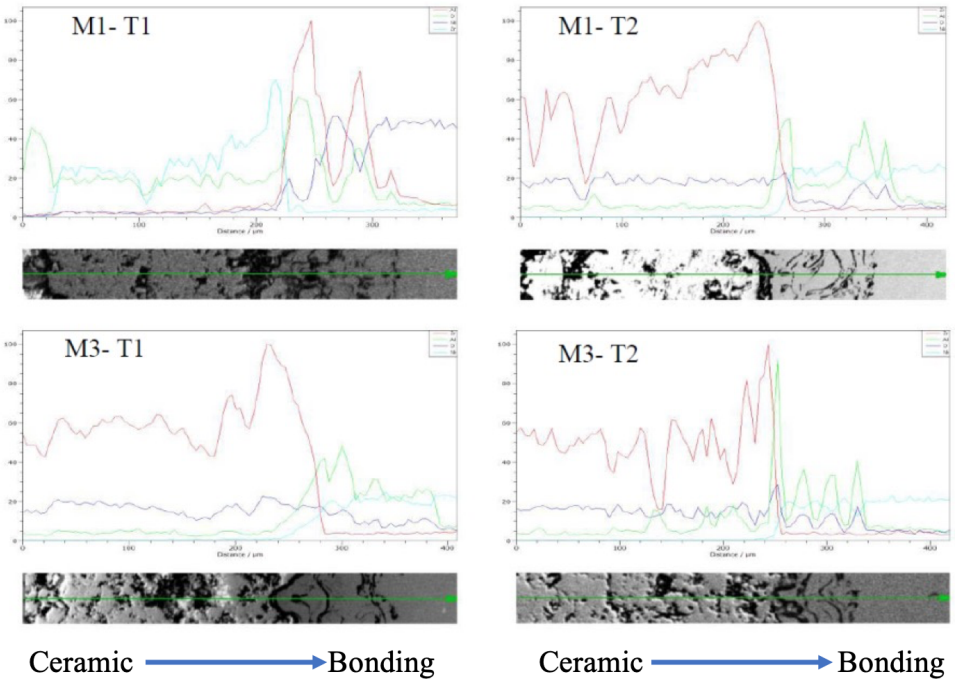

Fig. 8. Concentration profiles of the coatings by GDS.

Oxygen and aluminum concentrations were low at the bonding coating for the sample M3-T1, and when the aging time increased, the aluminum and oxygen concentrations increase at the ceramic-bonding interphase and reduce progressively into the bonding coating. These results show how the sample M3 had lower oxidation since the 100 h of treatment, and the thickness of the TGO at 700 h of treatment was lesser than the sample M1, which reported the maximum thickness gradient of TGO (Table 3).

3.3 Determination of the mechanical properties through nanoindentation

Typical graphs of load and unload during the nanoindentation test from the different coatings of the sample M1-T1are shown in Figure 9. For the ceramic coating, the area under the curve was small, and the maximum depth of the indenter was the smallest (0.4 μm) for the other layers. The TGO graph shows some deviations during the loading correlated with micro-cracks forming during the indentation, characteristic behavior of a brittle material, like the metallic oxides. The indenter's maximum depth was the highest value (0.9 μm) for the other layers. The bonding coat shows a typical graph of load and unloads with a maximum depth of 0.6 μm. The ceramic layer reported the highest hardness value for the bonding coating and TGO. Through nano-indentation tests, the Universal hardness (Martens), Young's modulus, and toughness from all samples' ceramic layers were determined.

A code to determine the corresponding values was elaborated in the MATLAB software (annexed hereto), to achieve a more straightforward and routine data handling. The TBC's manufactured by APS commonly show cracks splits, inter or outer splats, and interlamellar slides between them, representing inelastic deformations in the coating. The determination of Young's modulus is an important parameter to assess the quality of TBC's systems, and consequently, it is possible to predict the life span of such systems to establish a maintenance schedule for the engine and the blade. Figures 10 and 11 show the mechanical properties' values for ceramic coating of the TBC's (Toughness, Martens hardness, and Young's modulus, respectively). The toughness of ceramic coating (Figure 10) was inversely proportional to the argon flow. Samples with more argon flow (M1 and M2) reported less toughness than the samples M3 and M4, independent of aging time. Aging time and the projection distance does not have a clear tendency about the toughness because, in some cases, it increases or decreases.

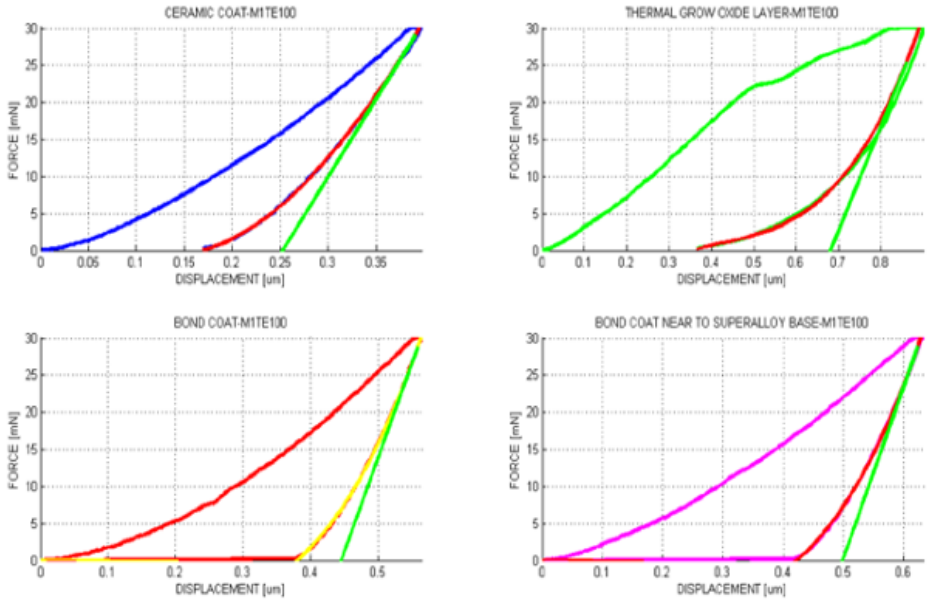

Fig. 9. Graphs of load and unload during the Nanoindentation test from the different coatings of the sample M1-T1.

In Figure 11, the highest hardness value corresponds to the sample M3 with 700 h of aging. The other samples' hardness decreased with the increase of the aging time, so the less argon flow (1.689 m^3/h) and more projection distance (82.55 mm) from the sample M3, reported the best hardness result. Usually, an increase of hardness represents a reduction in the toughness observed for the sample M3 in Figures 10 and 11.

The Young's Module in Figure 11 shows similar behavior to the toughness, where more argon flow (M1 and M2) correspond with less Young's Module and Toughness for the samples M3 and M4, with the difference that the aging time is proportional to Young's Module. The more aging time corresponds to an increase of Young's Module, the sample M3 that showed the best behavior.

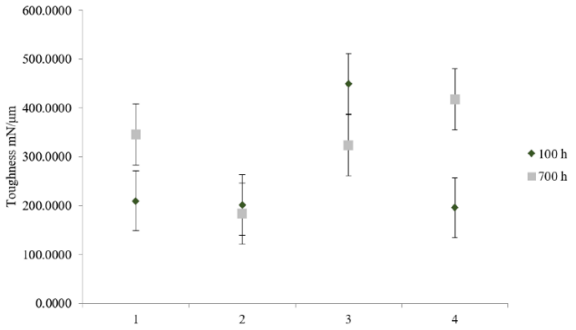

Fig. 10. Toughness values for ceramic coating in all assayed samples.

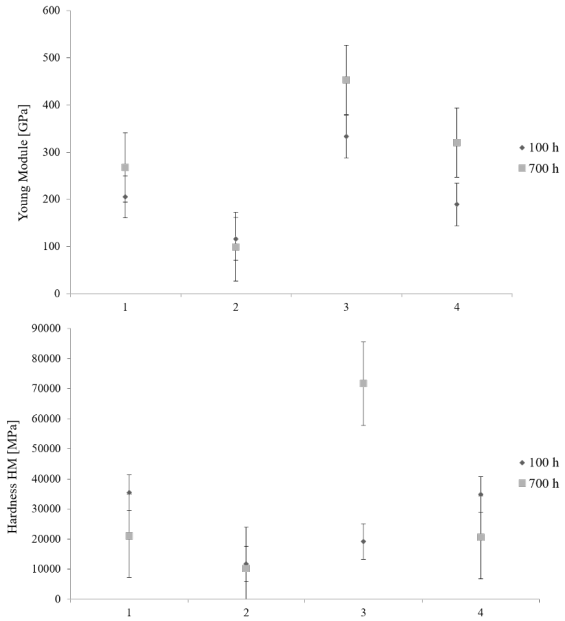

Fig. 11. Martens Hardness (down) and Young modulus (up) for ceramic coating in all assayed samples.

3.4 *Discussion*

In condition 1 (T1), the ceramic layer from the sample M3 reported the maximum thickness (335.2 μm). Thickest bonding layer (91.2 μm) corresponded to the sample M4, and the minimum TGO layer (5.5 μm) was observed in the sample M3.

Increase the aging time should be reflected in:

i) reduction of porosity and as a consequence, more coatings densification; ii) reduce of unmelt material and improve the adherence; iii) recovery, recrystallization and phase transformations that modify the mechanical properties and iv) diffusion of some elements toward he zones with less concentration to react with other elements if the thermodynamical conditions are favorable. In this sense, the expectation was to know how the argon flow and the projection distance affect improving the above characteristics to ensure consistency of each coating and obtain the minimum layer of TGO to reduce the bonding's fragility coating.

The smallest gradient between conditions 2 and 1 (T2 - T1) for the different layers (Table 3) is an essential condition that reflects the TBC's quality. The ceramic layer's minimum thickness gradient was -69.6 μm from the sample M3, which means that the lower argon flow (1.698 m^3/h) and higher projection distance (82.55 mm) were the best process condition for the ceramic coating. The minimum thickness gradient of the bonding layer was -6.7 μm from the sample M1, where the higher argon flow (1.981 m^3/h) and higher projection distance (82.55 mm) were the best process condition for the bonding coating. Although the better process conditions allow us to obtain more compact ceramic and bonding layers, the conditions that have the greatest effect in reducing the formation of TGO were a compact ceramic layer that prevents the passage of oxygen and a porous bonding layer that reduce aluminum diffusion.

The minimum thickness gradient of the TGO layer was 1.9 μm from the sample M3 with the minimum difference for the ceramic coating and intermediate gradient for the bonding coating. Concentration profiles by GDS technique from the samples M1 and M3 (Figure 8) showed how for the sample M1, the oxygen and aluminum concentrations are concentrated, and the bonding layer with 100 h of treatment. In the condition T2, the O_2 and Al concentrations were slightly reduced although they are still present in the bonding layer's width. Thermodynamically, the O_2 and Al are not limited to reacting until getting the interphase between the ceramic and bonding coatings, forming a concentration line, as shown in Figure 7. Aluminum diffusion of the bonding coating and their reaction with the oxygen to form Al_2O_3 in the ceramic-bonding interphase is an oxidation barrier that protects the substrate. Nevertheless, it produces embrittlement in the bonding coating and high risk of coating detachment. M3 sample, as the comparison, shows in the condition T1 a lesser oxygen concentration in the bonding layer. More aging time in the condition T2, both Al and O_2, are concentered in a thin oxidation line (TGO) in the ceramic-bonding interphase. The rest of the aluminum is present in the bonding coating, so not all aluminum is concentrated in the formation of TGO.

Hardness and Young's Module highest were reported in the ceramic layer of the sample M3. These results correspond with the best consistency of the coating during the Atmospheric Plasma Spray deposition. The lower argon flow of 1.698 m^3/h and the higher projection distance of 82.55 mm were the optimum parameters for the deposition of a TBC's by APS technique; obtaining a thin layer of TGO after a long exposition time by 700 h at 1000 °C

Conclusions

TBCs are technologies that have proven their usefulness for decades. However, the quality has not been cleared yet; in this research, we propose a first approach that relates manufacturing with the quality criteria for a TBC.

More densification of the ceramic coating is an essential factor in reducing the oxygen's presence toward the bonding coating. Know the deposition parameters that permit the diffusion and porosity reduction of the ceramic coating, offer the oxidation protection of the bonding coating, as was observed in the sample M3.

Embrittlement of the bonding coating can be reduced through control of the aluminum diffusion toward the ceramic-bonding interphase. This diffusion can be controlled with the deposition of optimum particles in size and morphology that permit some level of porosity and thermal stability of the bonding coating, as it was the sample M3. Hence, aluminum diffusion to lower concentration areas could be reduced, and with this, the control in the formation of a thin TGO layer. Avoid high concentration gradients of aluminum in the bonding coating to improve the bonding coating's thermal fatigue.

Acknowledgements

All the authors gratefully acknowledge support obtained by CONACYT, CONCYTEQ and

our institutions (UTEQ, CIDETEQ, UNAQ, CINVESTAV-QRO., UPSRJ, CIDESI, and CENAM).

References

Armengol González, S. (2006). *Caracterización Microestructural y Mecánica de Barreras Térmicas por APS y EBPVD Degradados por Fatiga Térmica y Por Contacto*. Tesis Licenciatura. Universidad Politécnica de Cataluña, 1-19.

Chen, W.R., Wu, X., Marple, B.R. (2006). The growth and influence grown oxide in a thermal barrier coating. *Surface and Coatings Technology 201*, 1074-1079. https://doi.org/10.1016/j.surfcoat.2006.01.023

Clarke, D. R., Oechsner, M., Padture, N. (2012). Thermal barrier coatings for more efficient gas turbine engines. *MRS Bulletin 37*, 891-898. DOI: https://doi.org/10.1557/mrs.2012.232

García Martínez, M. (2013). *Desarrollo de Recubrimientos de Base Aluminio Mediante "MOCVD" Para Protección Frente a La Corrosión y a La Oxidación.* Tesis Doctorado. Universidad Complutense de Madrid. 209-213.

Levi, C.G. (2003). Materials design for the next generation thermal barrier coatings. *Annual Review of Materials Research 33*, 383-417. https://doi.org/10.1146/annurev.matsci.33.011403.113718

Manning Meier, S., Nissley, D. M. & D. K. (1991). *Thermal Barrier Coating Life Prediction*. ASME. Ed. New York, N.Y 91-GT-40. 10017.

Miller, R.A. (1984) Oxidation-based model for thermal barrier coating life. *Journal of the American Ceramic Society 67*, 517-521. https://doi.org/10.1111/j.1151-2916.1984.tb19162.x

Ramírez-Hernández, A., Valera-Zaragoza, M., Aparicio-Saguilán, A., & Conde-Acevedo, J. (2020). Thermal behavior of banana starch films with degraded polyethylene terephthalate. *Revista Mexicana de Ingeniería Química 14*, 513-521. http://rmiq.org/ojs311/index.php/rmiq/article/view/1290

Reed, R. C. (2008). *The superalloys: Fundamentals and Applications*. Book Cambridge University Press.

Salgado-Delgado, A., Vargas-Galarza, Z., Salgado-Delgado, R., García-Hernández, E., Hernández-Díaz, W.N., Rubio-Rosas, E. and Salgado-Rodríguez, R. (2020). Morphological and thermal characterization of a high porous composite of biomaterial phema-chitosan-ceramic (hydroxyapatite). *Revista Mexicana de Ingeniería Química 15*, 625-632. http://rmiq.org/ojs311/index.php/rmiq/article/view/1239

Schweda, M.; Beck, T.; Malzbender, J.; Singheiser, L. (2015). Thermal cycling damage evolution of a thermal barrier coating and the influence of substrate creep, interface roughness and pre-oxidation. *International Journal of Materials Research 103*, 40-49. https://doi.org/10.3139/146.110627

Stecura, S., Leibert, C.H. (1977) U.S. Patent No. 4,055,705. Washington, DC: U.S. Patent and Trademark Office.

Tsipas, S.A., Golosnoy, I.O., Clyne, T. W., Damani, R. (2004). The effect of a high thermal gradient on sintering and stiffening in the top coat of a thermal barrier coating system. *Journal of Thermal Spray Technology 13*, 370-376. https://doi.org/10.1361/10599630420380

Vine, R.W.; Sheffler, K.D.; Bevan, C.E. (1989) U.S. Patent No. 4,861,618. Washington, DC: U.S. Patent and Trademark Office.